Spring 3-28-2024

A Comparison of Beamforming Characteristics in Isotropic and Composite Plate Structures for use in Structural Health Monitoring

Sarah Ketchersid
Embry-Riddle Aeronautical University, ketchers@my.erau.edu

To my nephew, I hope this inspires you to reach for the stars.

ACKNOWLEDGEMENTS

First and foremost, I want to thank my advisor, Dr. Daewon Kim, without whom's support and expertise I could not have completed this research. I also want to extend my gratitude to my committee, Dr. Shirish Namilae and Dr. Yizhou Jiang. Thank you for your support, feedback, and suggestions. This work is better with your help. A sincere thank you to Professor Travis Billette in the Aviation Maintenance Science Department for allowing my access to his facilities and his expertise in carbon fiber manufacturing. I could not have made my own composite laminate without your help. Thank you for your advice in the process and all of your valuable assistance.

Thank you to the professionals and donors of materials at Continuous Composites, Inc and Adhesive Prepregs for Composite Manufacturers (APCM) whose materials supported this work.

A sincere thank you to Taylor Stark, whose experience in similar work provided the groundwork for this research. Additionally, Taylor's continued support when I had questions about the equipment and processes were monumentally helpful.

Finally, I want to thank my closest friends, families, and colleagues. Working fulltime while fulling this thesis has been one of the hardest things I've had to do in my life. Without your encouragement and support, I would not be where I am today.

And to my fiance, Alex, thank you for always allowing me to put my studies first, providing much needed distractions when stresses were high, and letting me complain endlessly when my scans were taking way too long. I love you.

ABSTRACT

Structural health monitoring in plate-like simple structures using phased array beamsteering of guided Lamb waves is useful in damage detection and evaluation efforts. Lamb waves can be effectively used for beamsteering using a linear array. The experimentation primarily focuses on beamsteering in the aluminum panel, which involves developing a simulation based on extracted data to visualize the dispersion of waves across the panel. By evaluating parameters such as slowness, velocity, and amplitude direction and variation for a specific metallic plate, the wavefront generated by a single wave source can be represented as a function of propagation angle and distance from the origin. Using the aluminum panel as the baseline for an established process, the same methodology is extended to the quasi-isotropic panels, where both the Additive Manufactured and conventional composite laminates have a layer sequence of $[45/-45/90/0]_s$. Given the inherent anisotropy of composite materials, the propagation of guided waves varies with direction, resulting in a non-circular wavefront. The time delays for the composite cases are experimentally determined based off the algorithm developed for aluminum cases. Anisotropic waveforms can be effectively utilized for beam steering in specific directions with a linear piezoceramic array, achieving performance comparable to the isotropic case.

Additional testing was completed with a simulated crack in the plate. Using the same experimental methods, a 3D model was created showing the refraction of the wave at the point of damage. This additional testing demonstrates the success and usefulness of the linear PZT array in structural health monitoring and damage detection methods.

TABLE OF CONTENTS

LIST OF FIGURES

LIST OF TABLES

1 Introduction

Given the extensive use of composites across various industries, particularly in mechanical and aerospace domains, ensuring the safety and durability of composite applications becomes paramount. Industries are rapidly changing as they move to additive manufacturing processes, including carbon fiber printing. With new methods comes new challenges in damage detection and evaluation. Damage detection plays a critical role in Structural Health Monitoring (SHM), particularly in the aerospace industry, where the integrity of structures is paramount for safety and operational efficiency.

Damage detection allows maintenance crews and engineers to identify and address structural issues promptly, minimizing the risk of in-flight incidents or accidents. Timely detection and assessment of damage enable proactive maintenance strategies, such as repair or replacement of damaged components during scheduled maintenance intervals, thereby reducing downtime and operational disruptions. This proactive approach to maintenance also helps extend the lifespan of aerospace structures and optimize maintenance costs.

Various mechanisms can lead to damage in composite materials. Fatigue over time and the spread of damage from impacts, which might not manifest as surface damage that can be visually detected, can result in delamination of underlying layers. Unlike metals, identifying damage propagation or occurrence visually is challenging in composites, necessitating alternative detection methods.

Throughout this thesis, the author will delve into the promising technique of utilizing phased array beamsteering of guided Lamb waves for SHM in plate-like structures, focusing on its potential for detecting and evaluating damage.

1.1 Structural Health Monitoring

Structural Health Monitoring has emerged as a critical technology in the field of aviation, revolutionizing the way aircraft safety and maintenance are approached. In the dynamic and demanding world of aviation, where passenger safety is paramount, the structural integrity of an aircraft is a top priority. SHM plays a pivotal role in ensuring that aircraft remain in optimal condition throughout their operational lifespans.

Aviation has come a long way since the Wright brothers' first powered flight in 1903. Today, the skies are filled with a vast array of aircraft, ranging from small private planes to massive commercial airliners and military jets. These aircraft are subjected to a wide range of stresses and environmental conditions, from turbulence and extreme temperatures to the forces generated during takeoff and landing. Over time, these factors can lead to wear and tear on an aircraft's structure, potentially compromising its safety.

This is where Structural Health Monitoring steps in. SHM is a comprehensive system that employs a combination of sensors, data analysis, and predictive algorithms to continuously assess the condition of an aircraft's structure. It provides real-time data on the integrity of critical components such as the wings, fuselage, landing gear, and engine mounts. By monitoring these key structural elements, SHM enables early detection of defects, cracks, corrosion, or other anomalies that may compromise the aircraft's safety.

The benefits of SHM in aviation are numerous. First and foremost, it enhances safety by identifying potential issues before they escalate into major problems. This proactive approach to maintenance reduces the risk of catastrophic failures in flight, thus ensuring the well-being of passengers and crew. Additionally, SHM can extend the operational life of aircraft, optimizing their efficiency and reducing the overall cost of ownership for airlines and operators. SHM contributes to sustainability efforts in aviation by enabling more precise maintenance schedules

and reducing the need for unnecessary inspections and repairs, helping decrease the environmental impact of aviation by conserving resources and reducing waste.

This introduction merely scratches the surface of the vast and evolving field of Structural Health Monitoring in aviation. As technology continues to advance, the capabilities of SHM systems will only grow, making aviation safer, more efficient, and more sustainable. In this era of innovation, the continued integration of SHM into the aviation industry promises to play a pivotal role in shaping the future of flight.

1.1.1 Structural Health Monitoring versus Non-Destructive Testing

Structural Health Monitoring and Non-Destructive Testing (NDT) are two crucial techniques employed in assessing the condition and integrity of structures, each offering distinct advantages. While NDT has long been a staple in detecting defects and anomalies in materials without causing damage, SHM presents a dynamic approach by continuously monitoring structures for signs of damage or degradation over time.

The benefits of SHM over NDT are notable. Unlike traditional NDT methods which typically provide a snapshot of a structure's condition at a specific point in time, SHM offers real-time or periodic monitoring, allowing for the detection of subtle changes or evolving damage mechanisms because sensors are embedded and autonomously assessing structures in real time. This continuous monitoring capability enables early detection of damage, facilitating timely maintenance or repair interventions before catastrophic failures occur, and allows for the prediction of the remaining useful life of the product.

SHM systems can provide a wealth of data over an extended period, enabling engineers to analyze structural behavior, predict future performance, and optimize maintenance schedules more effectively. This proactive approach to asset management can result in cost savings by extending

the lifespan of structures and minimizing downtime. Additionally, SHM techniques often integrate advanced sensor technologies, such as accelerometers, strain gauges, or fiber optic sensors, offering higher sensitivity and spatial resolution compared to conventional NDT methods. This enhanced sensitivity allows for the detection of smaller defects or anomalies, providing a more comprehensive assessment of structural health. SHM systems can be implemented remotely or autonomously, reducing the need for manual inspections and enhancing safety, especially in hazardous or hard-to-reach environments. By minimizing human intervention, SHM also mitigates the risk of human error and ensures consistent and reliable monitoring outcomes.

There are many useful methods for SHM and NDE, such as electrical impedance, fiber optic sensors, microelectromechanical systems (MEMS) accelerometers, acoustic emissions, and ultrasonics. Ultrasonics and radiography involve applying energy to the structure and observing its response using piezoelectric transducers and X-rays. NDE techniques often focus on evaluating through-thickness properties. However, the propagation of guided Lamb waves within the plane of plate structures presents a particularly intriguing avenue for SHM systems.

While NDT remains a valuable tool for assessing the integrity of structures, active SHM offers distinct advantages in terms of real-time monitoring, early damage detection, data richness, sensor capabilities, remote deployment, and overall safety. As technology and research continues to advance, the integration of SHM into structural management practices is expected to become increasingly prevalent, contributing to safer, more resilient, and cost-effective infrastructure systems.

1.1.2 Application of Piezoelectic Materials in SHM

There have been numerous studies on the integration of a piezoelectric wafer-based structural health monitoring system embedded in structures [1-10]. The main objective of these studies is to enhance the identification of flaws and deformations in structures in real time. Piezoelectric (PZT)

sensors and actuators are indispensable components in SHM due to their remarkable properties and capabilities. PZT sensors, renowned for their high sensitivity to mechanical vibrations and deformations, excel at detecting even the slightest structural changes like cracks and fatigue, making them invaluable for early damage detection. Additionally, PZT sensors are incredibly versatile, capable of monitoring a wide range of structures across various industries, from civil infrastructure to aerospace and automotive applications.

PZT actuators complement sensors by generating controlled mechanical vibrations or deformations, facilitating active SHM techniques and in-situ inspections. Their ability to operate at high frequencies is crucial for Lamb wave-based inspections and damage characterization. Moreover, PZT sensors and actuators are non-invasive, meaning they can be attached to structures without causing damage, making them suitable for retrofitting existing systems and structures while ensuring minimal disruption. Their real-time monitoring capabilities enable immediate responses to structural changes, which is crucial for industries prioritizing safety, such as aerospace and civil engineering. Scalability and network integration round out the list of benefits, allowing PZT sensors to be easily adapted to large structures and integrated into centralized monitoring systems, providing comprehensive SHM coverage and improved structural integrity.

Over the past few decades, extensive research has been conducted on lead zirconate titanate (PZT) piezoelectric transducers and their various applications [5, 6, 11-16]. In one study, Boukabache *et al.* [17] used the pitch-catch principle to detect defects and deformations in aircraft structures. The principle involves transmitting guided waves from one PZT to another, with the damaged area between the sensors inducing impedance in the wave, leading to reflection and refraction. The resulting impedance is caused by scattering in all directions when the wave hits a point in the material where the material properties change. This change is then considered and

processed to identify defects and deformations in the structure itself [18]. However, one limitation of this deformation and damage detection method is the requirement of deploying a large number of sensors around the structure to ensure comprehensive coverage of the detection area. To address this complexity, an alternative approach involves utilizing an array of PZTs and employing beamforming techniques to steer the generated beams and effectively scan a wide structural area. [9, 137.

1.2 Guided Lamb Waves

Guided Lamb waves, often referred to simply as Lamb waves, are a type of guided ultrasonic wave that propagates through thin plate-like structures, such as those commonly found in aircraft components. They are named after the British mathematician Horace Lamb, who described them mathematically in the early 20th century. Guided Lamb waves can be induced and detected through various methods. Researchers have explored Piezoelectric (PZT) and MacroFiber Composites (MFC) actuators, fiber optics, Electromagnetic Acoustic Transducers (EMATs), Magnetostrictive sensors, Adaptive Frequency Control (AFC), SMART layers, among others [1-23]. PZT actuators and similar technologies show particular promise as they can serve both as actuators and sensors, reducing the number of components needed and enabling monitoring of entire structures with minimal actuators. Researchers have investigated different sensor configurations, with various approaches outlined in a comprehensive overview by Lissenden and Rose [19]. One system involves beamsteering using a central linear phased array of actuators, which is the focal point of this work.

Lamb waves are elastic waves that travel along the thickness of a solid plate while interacting with its surfaces. A single structure can theoretically support numerous Lamb wave modes, typically categorized into symmetric (extensional) and antisymmetric (flexural) types. They

propagate in a dispersive manner, meaning their velocity depends on both frequency and thickness of the plate.

One of the key advantages of Lamb waves is their sensitivity to various types of defects, such as cracks, delamination, corrosion, and voids within the plate. When Lamb waves encounter a defect, they reflect, scatter, or change their mode, making it possible to detect and characterize these flaws accurately. Lamb waves can cover a relatively large area of the structure under examination from a single sensor location, making them efficient for inspecting large aerospace components like wings, fuselages, and engine components.

Numerous contemporary SHM systems employ Lamb waves to detect and identify damage in both composite and metallic configurations. Lamb waves offer a significant advantage in any material by traversing long distances with minimal amplitude loss [13]. Consequently, a wide area can be monitored using only a handful of sensors. Unlike traditional NDE methods, Lamb waves enable the detection of damage even when it's not proximate to the sensors.

Lamb wave-based monitoring can be adapted for both on-ground inspections during maintenance and in-flight monitoring through embedded sensors, enabling continuous health monitoring of aircraft structures. By using Lamb waves, aerospace professionals can often perform inspections without the need for disassembling the entire aircraft, reducing maintenance downtime and costs. Lamb wave data can be processed and analyzed quantitatively, providing information about the size, location, and severity of defects. This data aids engineers and technicians in making informed decisions about repairs and maintenance. In addition to inspection and testing, Lamb waves are valuable for research and development purposes in the aerospace industry. They can be used to study the behavior of composite materials, validate structural designs, and improve the understanding of wave propagation in complex structures. In summary, guided Lamb waves are a

valuable tool in the aerospace industry's toolkit. Their ability to efficiently inspect large, complex structures, detect defects early, and provide quantitative data makes them essential for ensuring the structural integrity and safety of aircraft components.

The dispersion curves illustrate the relationship between frequency and velocity for the different modes, which will be discussed further in later sections. In isotropic plates, dispersion is solely influenced by material properties, with straightforward derivations from 3D elasticity theory. However, determining valid wave modes requires numerical methods due to complexity [13]. For anisotropic materials, dispersion properties vary directionally and can't be assumed constant. Despite added complexity, dispersion interactions for composite materials can be numerically found using 3D elasticity or higher-order plate theory and equations of motion, as demonstrated by Wang, et al. [1]. Alternatively, they can be determined experimentally [2] or through finite element methods [3].

1.3 Phased Array Beamforming

Traditionally, NDT techniques relied on fixed transducers or probes that emit waves in a single direction. However, these methods have limitations in terms of their ability to thoroughly inspect complex components and structures. This is where SHM methods phased array beamsteering steps in. At its core, it involves an array of individual ultrasonic transducer elements, each of which can be electronically controlled in terms of phase and amplitude. This control allows for the manipulation of the ultrasonic beam in real-time, offering several advantages for SHM applications.

One of the primary advantages of phased array beamsteering is its ability to dynamically control the direction and focus of ultrasonic waves without physically repositioning the transducer. This capability is particularly valuable when inspecting intricate or curved surfaces, where traditional fixed probes may miss critical areas. Phased array systems can adapt their beam angles

and focal points to ensure comprehensive coverage and precise defect detection. It relies on multiple actuators to shape a concentrated beam. In SHM, this capability facilitates pinpointing the precise location of damage relative to the sensor/actuator array. Using as little as four actuators, a directed beam can be generated in any desired direction by actuating them in a specifically determined sequence with varying time delays. The steered beam results from constructive wave interference.

The real-time adjustability of phased array beamsteering allows for superior flaw detection and characterization. By fine-tuning the ultrasonic beams, scanning the structure can achieve better resolution and accuracy in identifying defects such as cracks, voids, and delaminations within materials and structures. This leads to more reliable assessments of the structural integrity and quality of components, reducing the risk of unexpected failures. Phased array beamsteering also improves inspection efficiency. Unlike traditional methods that require manual adjustments or multiple scans from different angles, phased array systems can perform complex inspections rapidly and repeatedly over long distances. This speed not only reduces inspection times but also minimizes downtime in industry.

Beamsteering technology finds versatile applications across industries, facilitating precise and efficient SHM of critical assets. In aerospace, beamsteered SHM is integral to inspecting aircraft components like wings and fuselage, ensuring safety by detecting hidden defects early. Civil engineering benefits from beamsteering by continuously monitoring infrastructure such as bridges and buildings, mitigating risks posed by structural deterioration. In the renewable energy sector, wind turbine blades are safeguarded through beamsteered SHM, optimizing maintenance schedules and maximizing energy production. Marine industry applications encompass the inspection of ship hulls and offshore structures, while automotive manufacturing relies on

beamsteering for quality control of vehicle components. Rail transportation leverages beamsteering for monitoring railway tracks and infrastructure, enhancing safety and operational efficiency [2, 4, 6]. Lamb waves' ability to propagate over long distances with little wave dampening makes them well-suited for inspecting large and complex structures without the need for extensive sensor arrays, further enhancing their utility in beamsteering applications for SHM.

Phased array beamsteering enables comprehensive, accurate, and efficient inspections, ensuring that critical components and structures meet rigorous safety standards and implements the ability to use SHM methods for active and continuous monitoring where NDT methods are invasive or impractical. Phased array beamsteering has the potential to play an increasingly prominent role in SHM and NDT, offering new possibilities for improved materials testing, structural assessments, and quality control. Its adaptability and precision make it a key driver in enhancing the reliability and safety of infrastructure and products across a wide range of industries.

To accurately predict both the direction and shape of the main lobe and the additional side lobes of the beam, knowledge of wave propagation from each transducer is essential. In isotropic plates, omnidirectional point sources are generally assumed, with equal velocity and amplitude in all directions. Based on this assumption and using the delay and sum principle, Yu and Giurgiutiu developed a general beamforming method to predict the wave propagation generated by a linear phased array applied to an isotropic plate, validated through experiments [20].

Other phased array configurations, such as rectangular and circular arrays, have been proposed and investigated by researchers, resulting in more optimal beamforming with larger and narrower main lobes and smaller side lobes, desirable qualities for effective beamsteering [21, 22]. These two-dimensional arrays allow for a larger scope of monitoring. Where a linear array only has a useful range from approximately 60 to 120 degrees fore and aft, a 2D array will allow 360˚

monitoring of a structure. However, much of this research has been limited to isotropic materials, though there have been some recent advances in composite applications, such as CLOVER [11, 13].

An assumption of omnidirectional point sources is not always valid, and the beamforming algorithm previously established by Yu and Giurgiutiu may not be applicable in all configurations, including in isotropic mediums, as demonstrated by Kim and Philen's study on PZT and MacroFiber Composites (MFC) actuators, which exhibit anisotropic actuation [9, 10]. Because of the anisotropic properties of composite structures, similar challenges arise when attempting to apply the same beamforming principles to composite laminates.

As previously noted, the wave direction and speed within each layer are influenced by the angle between the beam and the fibers. Additional wave interactions occur at layer boundaries and are dependent on the angles between layers. In certain cases, particular frequencies may correspond to a mode where the slowness curve is nearly circular, allowing for the application of an omnidirectional source wave approximation. In such instances, a beamforming algorithm designed for isotropic plate structures can be employed.

In anisotropic composite laminates, it's unsuitable to assume a single point source as omnidirectional in a broad sense. The velocities and amplitudes of wave modes vary with direction and frequency, leading to non-circular wave fronts and complexity, particularly with specific wave modes.

1.4 Additive Manufacturing

Additive Manufacturing (AM), often commonly coined but not limited to 3D printing, has revolutionized traditional manufacturing processes by enabling the creation of complex geometries and customized components with unprecedented precision and efficiency. At its core, AM involves

the layer-by-layer deposition of material, allowing for the fabrication of intricate designs that are structurally robust directly from digital models [24].

One of the most promising advancements within the realm of AM is the integration of carbon fiber composites into the printing process. Carbon fiber AM marries the structural strength and lightweight properties of carbon fiber with the versatility and adaptability of additive manufacturing techniques. This fusion unlocks a myriad of possibilities across industries, ranging from aerospace and automotive to medical and consumer goods. The benefits of carbon fiber AM are manifold. It offers unparalleled strength-to-weight ratios, making it ideal for applications where weight reduction is critical without sacrificing structural integrity. This characteristic is particularly advantageous in industries like aerospace, where lightweight components translate to fuel efficiency and enhanced performance.

Carbon fiber AM enables the production of highly durable and corrosion-resistant parts, prolonging the lifespan of products and reducing maintenance costs. This durability, coupled with the ability to create complex shapes and intricate structures, opens new avenues for design innovation and optimization. Engineers can now push the boundaries of conventional manufacturing constraints, creating components with optimized geometries like complex lattices tailored to specific performance requirements [25, 26]. The additive nature of carbon fiber AM minimizes material waste compared to traditional subtractive manufacturing methods, resulting in cost savings and environmental benefits [24]. By precisely depositing material only where needed, manufacturers can optimize material usage and reduce overall production waste.

In addition to these tangible benefits, carbon fiber AM facilitates rapid prototyping and iteration, accelerating product development cycles and time-to-market. Designers and engineers can quickly test and refine concepts, reducing the lead time from the initial idea to the final product.

Carbon fiber additive manufacturing represents a transformative leap in manufacturing technology, offering unparalleled strength, lightweight properties, design flexibility, cost efficiency, and environmental sustainability. Already making waves in many industries, as the technology continues to evolve and become more accessible, its impact across all industries is poised to reshape the way we design, produce, and utilize products in the years to come.

2 Guided Lamb Waves

Guided Lamb waves are elastic waves present in thin, plate-like structures, where thickness is significantly smaller than other dimensions. These waves exhibit high dispersion in any solid material, meaning their velocity varies with frequency. Their movement is influenced by the physical boundaries of the plate, hence the designation of "guided" Lamb waves. The initial mathematical exploration and forecast of these waves in infinite plates dates back to 1917, pioneered and documented by Horace Lamb, where they derive their name. A similar guided wave phenomena was demonstrated to occur on the surfaces of semi-infinite solid objects by Lord Rayleigh in 1885. Because of their numerous similarities, these two wave types are frequently mentioned together as Rayleigh-Lamb waves. Additionally, Lamb wave theory has expanded to encompass tubes, shell structures, and curved plates. The subsequent sections of this chapter will delve into this issue specifically as it applies to simple plates.

Figure 2.1 Plate model and notationillustrates the problem schematic and the adopted notation. The x_3 axis aligns parallel to the plate surface, while the x_1 and x_2 axes lie within the plane, representing the primary material coordinate system, particularly in the context of anisotropic scenarios. Guided Lamb waves exhibit particle motion that takes place within the plane parallel to both the normal of the plate and the direction of propagation. For instance, for a wave traveling in the x_1 direction, this motion transpires within the $x_1 - x_3$ plane.

A notable characteristic of guided Lamb waves is the abundance of potential wave modes within a given medium. In a semi-infinite structure, only two bulk wave mode types are supported: dilatational (longitudinal/P-waves) and distortional (shear/S-waves). A finite plate, however, can sustain an infinite array of Lamb wave modes, with additional modes emerging simultaneously at higher frequencies.

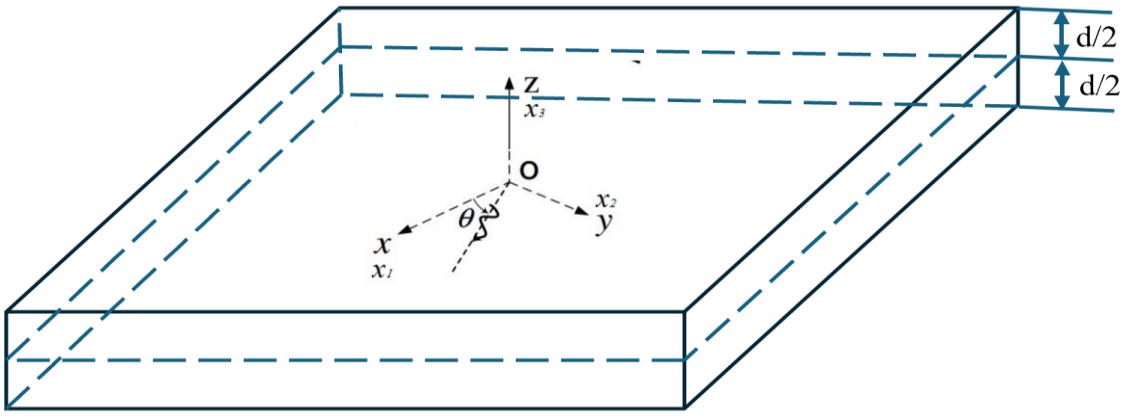

Figure 2.1 Plate model and notation

The prediction of Lamb wave motion can be derived from the general wave equation, as elaborated in later sections. In any given material, Lamb waves demonstrate varying degrees of dispersion in group and phase velocities with frequency across different wave modes. Section 2.1 provides a more detailed explanation of phase and group velocity concepts.

Broadly, Lamb wave modes can be categorized into two groups: asymmetric (or antisymmetric) and symmetric. This terminology refers to the out-of-plane particle motion concerning the mid-plane, as depicted in Figure 2.2. It's worth noting that actual particle motion is elliptical rather than strictly confined to out-of-plane displacement. Asymmetric modes exhibit a greater factor in the transverse x_3 direction, while symmetric modes tend to emphasize a larger factor parallel to the direction of wave propagation. This distinction is particularly significant for the primary zero-order modes. Consequently, these properties give rise to another name for the two classes of waves: extensional (symmetric) and flexural (asymmetric).

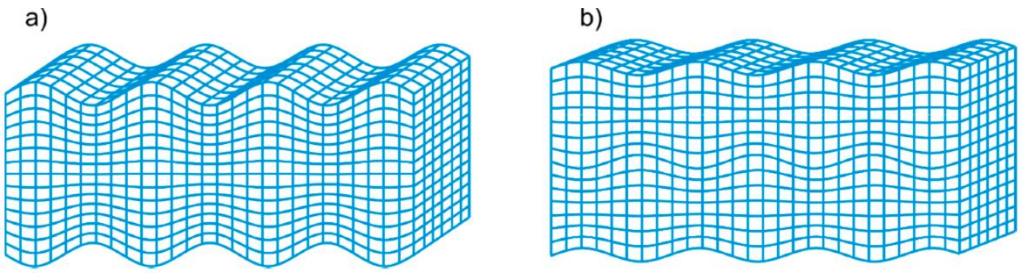

Figure 2.2 (a) Symmetric and (b) asymmetric guided Lamb wave modes [27]

Subsequent sections delve into further detail on guided wave concepts and discuss the governing equations of beamforming in both isotropic and anisotropic plates, derived from the 3D Elasticity Theory.

2.1 Phase and Group Velocities

When waves move through a medium, they demonstrate two discernible velocities. The group velocity signifies how quickly the entire wave envelope progresses through the medium, indicating the speed of the advancing wavefront. In contrast, the phase velocity indicates the rate at which individual wave peaks travel. Lord Rayleigh was one of the first to identify this distinction, stating, "when a group of waves advances into still water, the velocity of the group is less than that of the individual waves of which it is composed; the waves appear to advance through the group, dying away as they approach its interior limit" [28].

This quote describes a phenomenon known as wave dispersion. When a group of waves propagates into calm water, the speed at which the group moves forward is slower than the speed of the individual waves within the group. This disparity in velocities causes the individual waves to seem to move through the group, gradually diminishing as they approach the inner edge of the group, shown in Figure 2.3. In essence, this observation highlights the complex behavior of waves in a medium, where interactions between individual waves within a group result in an overall wave pattern characterized by variations in speed and intensity.

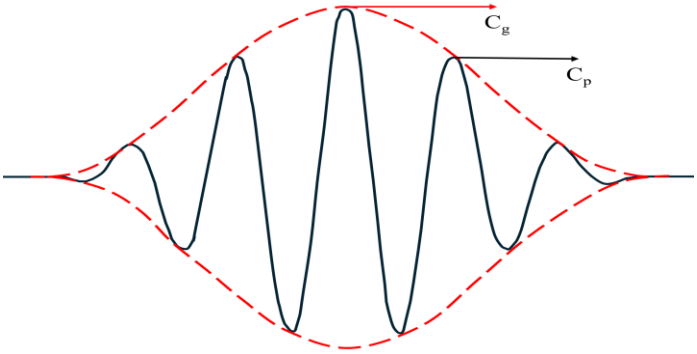

Figure 2.3 Group (C_g) and Phase (C_p) velocities of a wave packet

Several distinct scenarios can be observed. When the phase velocity aligns with the group velocity, the wave peaks remain static within the wave packet. Should the phase velocity surpass the group velocity, the waves seem to continually initiate from the start of the wave packet, traverse through it, and dissipate at the other end. Conversely, if the phase velocity falls below the group velocity, the waves appear to originate from the front of the wave packet and travel in the opposite direction of propagation, fading away at the wave packet's inception.

These scenarios arise in guided Lamb waves, with both velocities influenced by the thickness of the plate, the material properties, and the specific wave characteristics. Additionally, they are dispersive, and they vary across the ranges of frequency for each wave mode. The following sections offer derivations of the governing equations for phase and group velocities.

2.2 Dispersion Curves

Dispersion curves illustrate how the phase and group velocities and frequency relate across both symmetric and asymmetric modes. The term “dispersion” arises from the variation in both the group and phase velocity of a particular mode with frequency. Therefore, as a wave packet moves through the plate, it appears to spread because the frequency components propagate at different velocities. Figure 2.4 presents an example of dispersion relations in an aluminum plate.

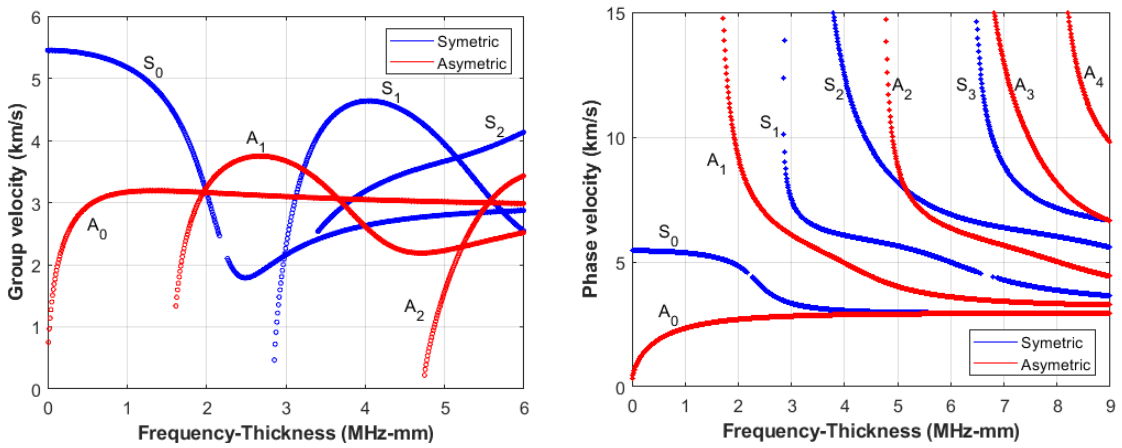

Figure 2.4 Dispersion curves for an isotropic aluminum panel (E=73.1 GPa, ν=0.33, ρ=2780 kg/m^3) [9]

In an isotropic plate, dispersion relations are determined solely by material properties and can be straightforwardly calculated using 3D elasticity theory. However, when dealing with composite materials, beamsteering becomes more complex. Factors such as the number and relationship/bonding between layers, the fiber direction and orientation, and the angle between propagating waves all affect the magnitude and the speed of wave propagation through the laminate. Consequently, these variables influence dispersion, leading to unique dispersion curves for various wave directions. The different wave modes described earlier may not be distinctly defined in composites and can exhibit significant coupling in some directions while showing little to no coupling in others.

2.3 Wave curves

In anisotropic plates, variations in material properties and stiffness matrices across different propagation angles θ impact both phase and group velocity. This effect can be observed through the plotting of "wave curves" in a polar coordinate system. A velocity curve illustrates the phase velocity vectors for various wave directions at a particular frequency within a given plate. The reciprocal of $1/C_p$, along with its plotted values, constitutes a slowness curve. Likewise, a wave

curve shows a representation of group velocity vectors on a polar plot. The group velocity vector at each point along the slowness curve is perpendicular to the tangent of the curve at that point. The angle between the group velocity vector and the corresponding phase velocity vector is defined as the "skew" angle. This occurrence is unique to anisotropic materials, with the skew angle serving as a physical representation of the direction of wave energy.

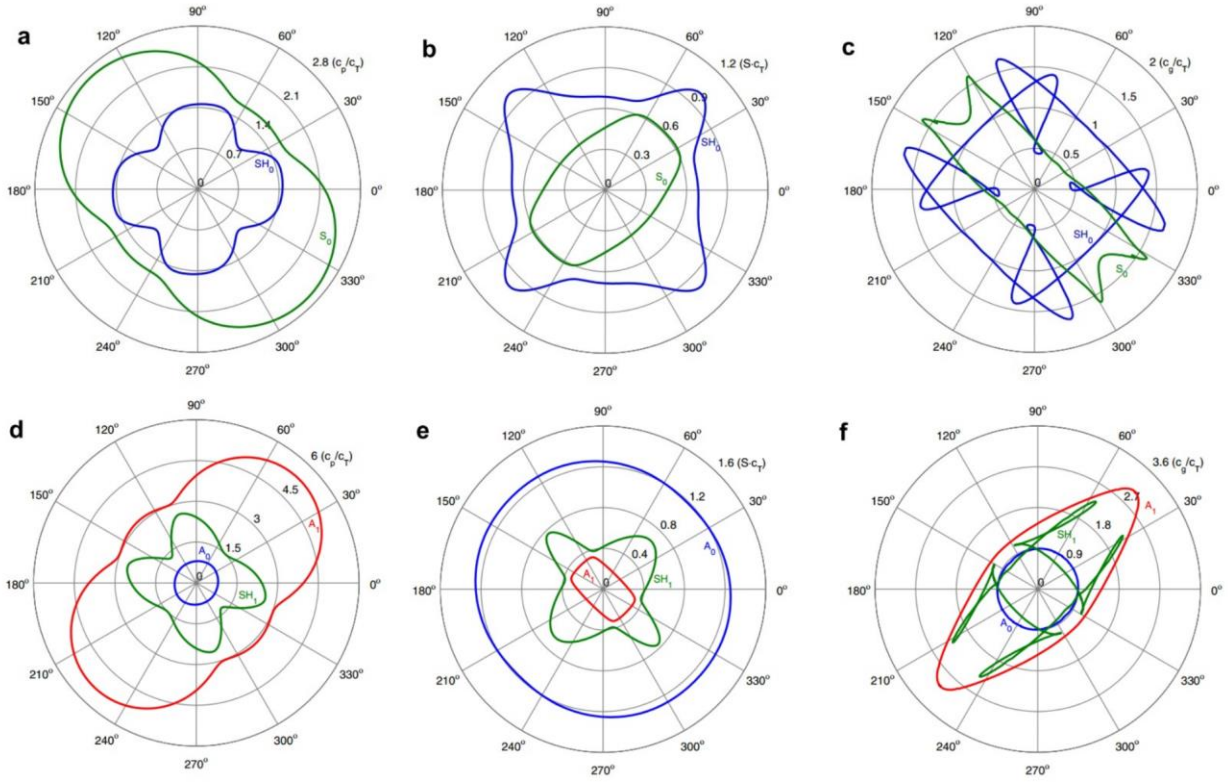

Figure 2.5 Velocity, slowness, and wave curves of Lamb waves in a [+45/-45]s laminate with a thickness of 3 mm: Symmetric modes (a) velocity curves; (b) slowness curves; (c) wave curves; and Asymmetric modes (d) velocity curves; (e) slowness curves; (f) wave curve [29]

The wave curve broadly portrays the shape of a wavefront originating from a single source located at the origin. In materials like aluminum that exhibit isotropic properties, the phase velocity, slowness, and wave curves typically manifest as circles, varying in magnitude across different frequencies and wave modes. However, in composites, these curves can become notably more complex. Figure 2.5 illustrates a selection of wave curves sourced from literature, depicting

the behavior of a 3mm thick $[+45/-45]_s$ composite plate at a frequency of 0.4MHz [29]. Although certain wave modes, such as A0 in this specific instance, may demonstrate nearly isotropic characteristics, this consistency is not universal across all wave modes. Furthermore, the A0 mode exhibits heightened influences of anisotropy within the same laminate but at varying frequencies.

2.4 Isotropic Material

The derivation of elastic beemsteering governing equations for isotropic plate materials can be found in many texts [13, 30, 31]. Starting with the Navier elasticity equation for a linearly elastic and isotropic material:

$$(\lambda + 2\mu)\nabla(\nabla \cdot u) - \mu\nabla \times (\nabla \times u) = \rho\ddot{u} \tag{2.1}$$

where μ and λ are Lamè constants. This statement represents displacement partial differential equations. The boundary conditions are free traction at both the top and bottom surfaces, expressed by:

$$\sigma_{31} = \sigma_{32} = \sigma_{33} = 0 \ at \ x_3 = \pm\frac{d}{2} \tag{2.2}$$

Using the method of potentials, the Navier elasticity equations results in two expressions using Helmholtz decomposition.

$$\frac{\delta^2\phi}{\delta {x_1}^2} + \frac{\delta^2\phi}{\delta {x_3}^2} = \frac{1}{{c_L}^2}\frac{\delta^2\phi}{\delta t^2}$$
$$\frac{\delta^2\psi}{\delta {x_1}^2} + \frac{\delta^2\psi}{\delta {x_3}^2} = \frac{1}{{c_T}^2}\frac{\delta^2\psi}{\delta t^2} \tag{2.3}$$

Assuming solutions (2.3) are in the harmonic wave form in the x_1-x_2 plane,

$$\begin{aligned} \phi &= \phi x_3 e^{i(\xi_1 x_1 + \xi_2 x_2 - \omega t)} \\ \psi &= \psi x_3 e^{i(\xi_1 x_1 + \xi_2 x_2 - \omega t)} \end{aligned} \tag{2.4}$$

where ξ_i is the wavenumber in the *i* direction, and ω is angular frequency. With mathematical alteration, the two decoupled governing equations relating the frequency and wavenumber for beamsteering guided wave modes is attained [13]:

$$\frac{tan(qh)}{tan(ph)} = -\frac{4k^2pq}{(q^2-k^2)^2} \qquad \text{Symmetric modes} \tag{2.5}$$

$$\frac{tan(qh)}{tan(ph)} = -\frac{(q^2-k^2)^2}{4k^2pq} \qquad \text{Asymmetric modes} \tag{2.6}$$

where the *p* and *q* terms are:

$$\begin{aligned} p^2 &= \frac{\omega^2}{{c_L}^k} - k^2 \\ q^2 &= \frac{\omega^2}{{c_T}^k} - k^2 \end{aligned} \tag{2.7}$$

All possible wave mode dispersion relations are defined by the governing equations. Real solutions are the roots of the expressions that can be found numerically, producing a range of combinations of phase velocities and frequencies corresponding to valid guided wave modes. Rose outlines a solution approach in his work [13] that can be utilized to find the desired solutions.

2.5 Anisotropic Material

The derivation for anisotropic material is much more complicated, due to the complexities of the material structure. Instead, the stress-strain relations are evaluated for a single layer, and then a partial wave method is utilized to achieve the governing equations. This derivation has already been completed by Osteric [32, 33], leaving the governing equations for a single layer:

$$D_{11}G_1 cot(\gamma\alpha_1) - D_{13}G_3 cot(\gamma\alpha_3) + D_{15}G_5 cot(\gamma\alpha_5) = 0 \qquad \text{Symmetric modes} \tag{2.8}$$

$$D_{11}G_1 tan(\gamma\alpha_1) - D_{13}G_3 tan(\gamma\alpha_3) + D_{15}G_5 tan(\gamma\alpha_5) = 0 \qquad \text{Asymmetric modes} \tag{2.9}$$

where,

$$\gamma = \frac{\xi d}{2} = \frac{\omega d}{2c_P} = \frac{\pi f d}{c_P}$$
$$G_1 = D_{23}D_{35} - D_{33}D_{25}$$
$$G_3 = D_{21}D_{35} - D_{31}D_{25} \quad (2.10)$$
$$G_5 = D_{21}D_{33} - D_{31}D_{23}$$

The roots of equations (2.8) and (2.9) correspond to real guided wave modes, and these roots can similarly be found using Rose's methods [13]. As material properties vary with the angle of wave propagation, it's necessary to repeat the process across a range of propagation angles, θ. The equations established in this section, however, are applicable solely to a single layer or a unidirectional composite layup, where the material characteristics remain consistent throughout the thickness of the laminate. When dealing with wavelengths significantly larger than the thickness of the laminate, the layering has negligible impact, and the laminate can be represented with averaged properties across its thickness [34-36]. To generalize the theory to encompass any composite layup, it is essential to solve the set of governing equations for each layer and ensure continuity at the boundaries between layers. Figure 2.6 illustrates an example of a multi-layered composite plate.

There are different approaches to formulating the multi-layer solution, especially adopting matrix methods. Lowe [37] and Kamal, *et al*. [38] gave thorough overviews of matrix techniques for wave propagation modeling. A brief overview of a few of the most popular approaches is given in the following subsections.

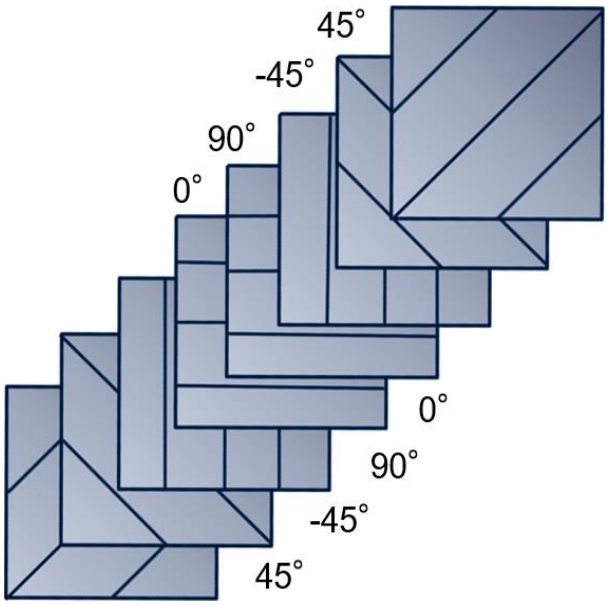

Figure 2.6 Schematic of an eight layer $[45/-45/90\text{-}0]_s$ quasi-isotropic composite laminate

2.5.1 Transfer Matrix Method

The transfer matrix method is a mathematical approach used to analyze wave propagation in layered structures, including composite materials. It involves representing each layer of the structure with a transfer matrix that describes how waves propagate through that layer. These transfer matrices are then multiplied together to obtain a global transfer matrix that represents the entire structure. By analyzing the properties of this global transfer matrix, such as its eigenvalues and eigenvectors, one can determine various characteristics of wave propagation, such as phase velocities, transmission and reflection coefficients, and mode shapes.

2.5.2 Stiffness Transfer Matrix Method

The stiffness transfer matrix method involves representing each layer of the composite as a transfer matrix that describes how waves propagate through that layer. These transfer matrices are then combined to form a global transfer matrix that represents the entire composite structure. By analyzing the eigenvalues and eigenvectors of this global transfer matrix, one can determine the

wave propagation characteristics, such as phase velocities and mode shapes, for different wave modes in the composite material.

2.5.3 Global Matrix Method

The global matrix method, also known as the global stiffness matrix method, involves assembling a global stiffness matrix that represents the entire composite structure by combining the stiffness matrices of individual elements or substructures. Each element's stiffness matrix describes its behavior under applied loads and boundary conditions. By solving the global stiffness matrix equation, one can determine the displacements and stresses throughout the composite structure, allowing for the prediction of wave propagation characteristics such as mode shapes and frequencies. This method is commonly used in finite element analysis to simulate wave propagation in complex composite structures with varying material properties and geometries.

2.5.4 Higher-order Plate Theory

The higher-order plate theory is a mathematical model used to describe the behavior of waves propagating in thin plates. Unlike simpler plate theories that assume constant stress and displacement distributions across the plate thickness, higher-order plate theories account for variations in these quantities through the thickness of the plate. These theories consider additional terms in the equations of motion to capture shear deformation effects and improve the accuracy of wave propagation predictions, especially in plates with non-uniform material properties or complex geometries. By incorporating higher-order terms, this theory provides a more realistic representation of wave behavior in thin plates, making it useful for analyzing wave propagation in composite materials and structures with curved or irregular shapes.

2.5.5 Semi Analytical Finite Element

Semi-analytical finite element methods combine the advantages of analytical and numerical techniques for analyzing wave propagation in structures. In these methods, the problem domain

is discretized into finite elements, similar to traditional finite element analysis. However, instead of solving the wave equations directly for each element numerically, semi-analytical methods use analytical solutions for some parts of the problem, while numerical techniques are applied to others. For example, in the context of wave propagation, analytical solutions may be used to describe the behavior of waves in simple regions of the structure, while numerical techniques are employed to handle more complex or irregular geometries. This hybrid approach allows for more efficient and accurate simulations of wave propagation compared to purely numerical methods, especially in cases where analytical solutions are available for certain portions of the problem. Semi-analytical finite element methods are commonly used in structural health monitoring and non-destructive testing applications to predict wave propagation behavior in composite materials and complex structures.

3 Phased Array Beamforming

Beamsteering involves the use of PZTs as actuators to produce wave beams within structures by exciting them at different time intervals [40]. This method employs multiple PZTs to superimpose Lamb waves constructively within the structure, creating a concentrated main wave lobe directed at the desired point. Lamb waves, elastic mechanical waves, are easily generated in plate structures and are confined by the plate surfaces. These ultrasonic waves propagate vertically between the surfaces of the plates. The wave velocity can be determined by knowing the frequency of the actuation signal and the plate thickness [40], seen previously in Figure 2.4. The characteristics of Lamb waves are influenced by factors such as excitation frequency, plate dimensions, and material properties [41, 42].

In isotropic or quasi-isotropic structures, it is generally assumed that wave propagation from excitation sources is uniformly circular. However, in beamforming scenarios, while the wave from planar arrays can be amplified towards a specific direction, it often produces minor side lobes propagating in other directions, complicating signal interpretation.

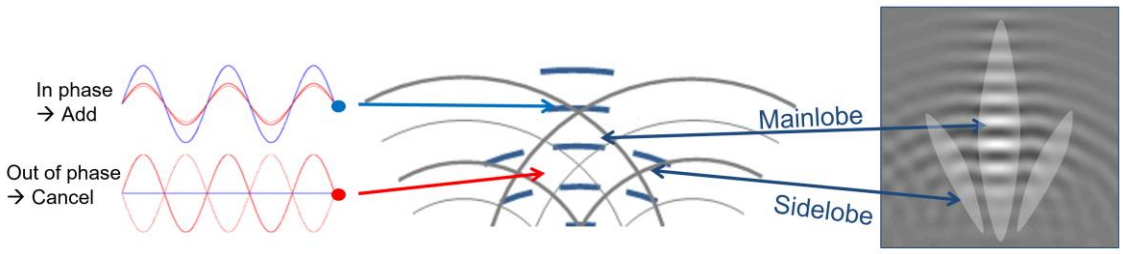

Figure 3.1 Beamforming through constructive and destructive wave interference [34]

Increasing the number of actuators in the array may be a solution, but this could be limited by physical constraints and the complexity of control electronics. Anisotropic materials like composite laminates exhibit faster and more efficient wave propagation along the direction of the fibers, with diminished strength when propagating orthogonally to the fiber direction [41, 42]. This

presents challenges in monitoring the structural integrity of anisotropic materials, such as composite laminates, compared to isotropic materials.

3.1 Near and Far Field

When assessing the response of phased arrays, it's crucial to distinguish between near-field and far-field conditions. In the far-field, wavefronts resulting from a point excitation can be represented as parallel planes, and individual rays can be considered parallel as well [21]. However, at distances closer to the array, this approximation becomes invalid, marking the transition into the near-field region. This condition for a particular array can be expressed as:

$$Near\ Field\ <\ d_f\ <\ Far\ Field \tag{3.1}$$

Where d_f is the Frauhofer distance. Defining D as the overall array size and λ as the signal wavelength, the Fraunhofer distance can be calculated as [38]:

$$d_f\ =\ \frac{2D^2}{\lambda} \tag{3.2}$$

3.2 Beamforming in Isotropic Case

To identify the location of damage, a proposed approach utilizes a time domain method involving multiple ultrasonic wave excitations. The positioning, amplitude, and phase shift of these excitations significantly impact the directionality and shape of the resulting beam [23]. These factors also vary depending on the location of the target.

To achieve efficient scanning, the wave must be targeted towards a specific angle. Steering of the ultrasonic beam is accomplished by exciting the PZTs at varying time intervals. Let Δm be the corresponding time delay related to M actuation positions. The time delay of an excitation is defined by:

$$\Delta_m = \frac{r}{c(\theta_T)} - \frac{r_m}{c(\theta_m)} \tag{3.3}$$

where, r represents the distance from the centroid of the excitation pattern to the target point, r_m is the distance for the excitation to the target point, $c(\theta_T)$ is the wave velocity in the propagation direction, θ_T, and $c(\theta_m)$ is the incident wave velocity from the actuation to the target, as shown in Figure 3.2.

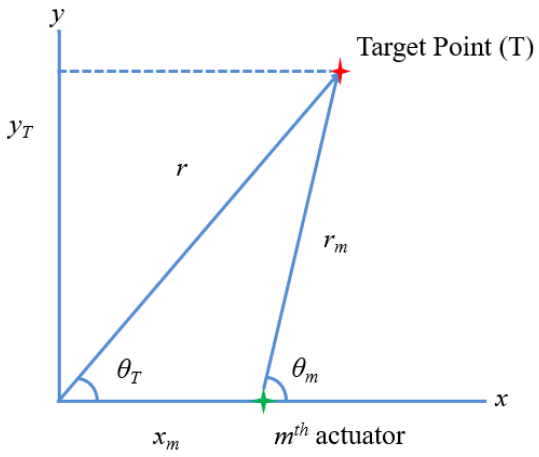

Figure 3.2 Near field schematic for a single actuation point and a target at θ_T direction.

Thus, the near field beamforming factor for a steered beam in an anisotropic medium becomes [23]:

$$BF(\theta)_{norm} = \frac{1}{M}\sum_{m=1}^{M} w_m \frac{1}{\sqrt{\frac{r_m}{r}}}\, e^{i2\pi f\left(\frac{r}{c(\theta_T)} - \frac{r_m}{c(\theta_m)} - \Delta_m\right)} \tag{3.4}$$

where f is the frequency and w_m is the weighting factor. Plugging Eq. (3.3) into Eq. (3.4),

$$BF(\theta)_{norm} = \frac{1}{M}\sum_{m=1}^{M} w_m \frac{1}{\sqrt{\frac{r_m}{r}}}\, e^{i2\pi f\left[\frac{r}{c(\theta_T)} - \frac{r_m}{c(\theta_m)} - \left(\frac{r}{c(\theta_T)} - \frac{r_m}{c(\theta_m)}\right)\right]} \tag{3.5}$$

Like r and θ_T, r_m and θ_m are annotated in Figure 3.2, and respectively written as:

$$r_m = \sqrt{(x_m - x_T)^2 + (y_m - y_T)^2} \tag{3.6}$$

$$\theta_m = \left| tan^{-1}\left(\frac{y_T - y_m}{x_T - x_m}\right)\right| \tag{3.7}$$

The isotropic theory represents a specific instance of the broader anisotropic principle. It employs a similar approach as described in the preceding section, albeit with simplifications in both phase velocity and amplitude. The discussion on isotropic beamforming has already been addressed by Yu, et al. [42]. In isotropic materials, wave propagation occurs irrespective of direction. The velocity and amplitude of the leading wave decrease solely with distance, influenced by dissipative forces arising from frictional molecular interactions among the vibrations generated within the material, thus:

$$c(\theta_T) = c(\theta_m) = c \quad \text{and} \quad w_m = 1 \tag{3.8}$$

Simplifying Eq. (3.5) by Eq. (3.8), the transformed beamforming expression becomes:

$$BF(\theta)_{norm} = \frac{1}{M}\sum_{m=1}^{M} \frac{1}{\sqrt{\frac{r_m}{r}}}\, e^{i2\pi f\left(\frac{r-r_m}{c}\right)} \tag{3.9}$$

The time delay Δ_m for a near field is given by:

$$\Delta_m = \frac{r - r_m}{c} \tag{3.10}$$

The amplitude and phase velocity in different directions are obtained from dispersion curves.

4 Experiment and Results

This experiment demonstrates the application of beamsteering using an array of four equally spaced PZTs to monitor beamforming characteristics of three 35 cm by 35 cm plates; (1) 2.03 mm thick aluminum 2024-T3 Clad plate, (2) 2.00 mm thick AM carbon fiber laminate with a 50% fiber volume fraction and acrylic resin, and (3) 1.00 mm thick conventional carbon fiber laminate plate fabricated with DA 4518U unidirectional carbon epoxy prepreg system with the same layup sequence as the printed sample, shown in Figure 4.1, with properties listed in Table 4.1.

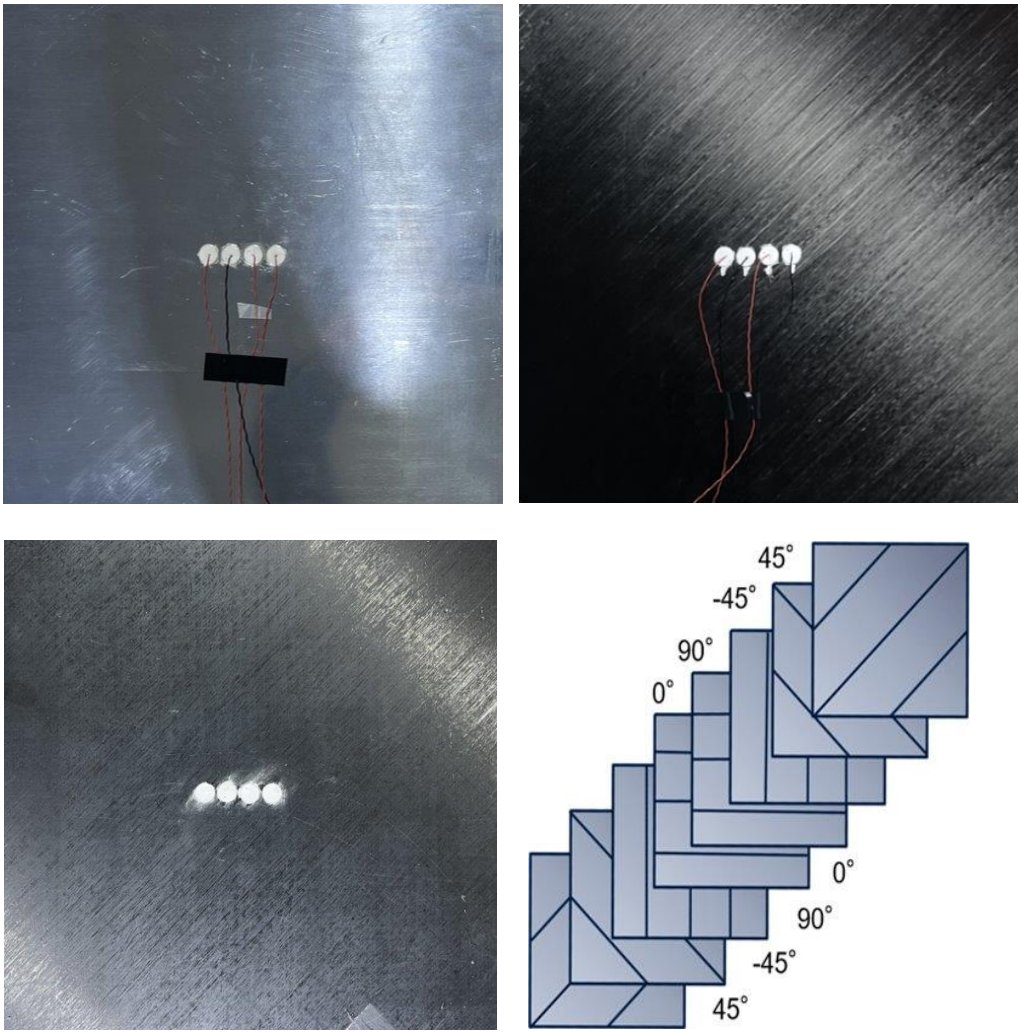

Figure 4.1 Aluminum plate; (b) AM composite; (c) conventional composite; (d) Both composite plates have the same layer sequence, $[45/-45/90/0]_s$. Four PZTs attached in array with 1.5cm between centers of adjacent PZTs.

Table 4.1 Materials and properties used.

	2024-T3C Aluminum	AM Composite	Conventional Composite
Thickness	2.03 mm	2.00 mm	1.00 mm
Dimensions	35 cm x 35 cm	35 cm x 35 cm	35 cm x 35 cm
Layup	N/A	$[45, -45, 90, 0]_s$	$[45, -45, 90, 0]_s$
Resin Content Post cure	N/A	50%	30%
Resin Type	N/A	Acrylic Resin	Epoxy Prepreg

The PZTs are attached to the plates in a specific arrangement, with one PZT positioned at the direct center of the plate and the remaining three PZTs evenly spaced, one on the right and two on the left of the center PZT. In each panel, MG Chemical's 8331D-14G silver conductive epoxy adhesive is used to attach the PZTs to the metal plate, serving as the negative terminal to complete the circuit for signal transmission to the PZTs. The PZTs are affixed to only one side of the plate, which coincides with the side where data is collected by the laser vibrometer.

4.1 Experimental Setup

For the aluminum panel, MATLAB is employed to compute the time delays for each PZT, considering the material and physical characteristics of the plate to achieve the desired beamsteered angle. Isotropic time delays are determined as a baseline for each case, with a target set at 10 cm from center. The same algorithm was used for each of the quasi-isotropic plates using the composite properties to find an initial time delay, and then experimentally tested and adjusted through iterations of testing.

The focus of observation and testing primarily lies in the top-right quadrant of the plate (quadrant I). Note that this discussion focuses on the 60° to 70° beamsteered angles for analysis and discussion. The calculated time delays are integrated into LabView code, and a 2.5 cycle

Hanning windowed sine signal is generated to excite each of actuator to cause beamforming wave propagation using the National Instruments NI PXIe-1071. The Hanning window was chosen due to its narrow band frequency content to minimize dispersion effects; a typical 2.5-cycles Hanning windowed sine excitation signal is shown below in Figure 4.2.

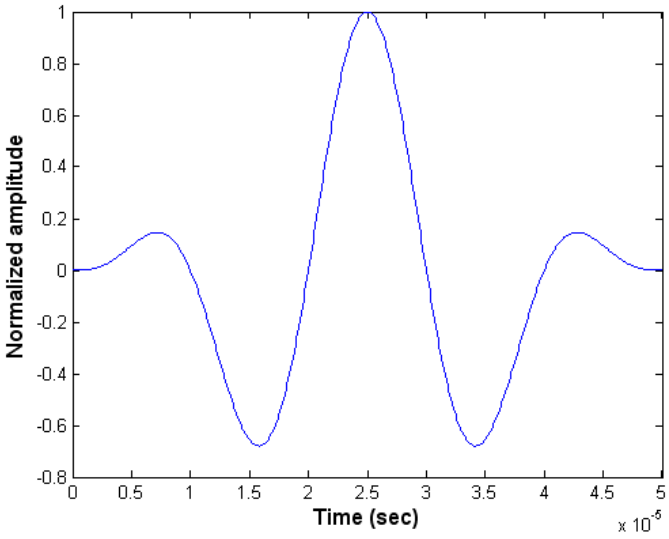

Figure 4.2 Typical 2.5-cycles Hanning windowed sine excitation signal

This signal is then transmitted to a National Instruments shielded connector block, from which it is passed through shielded connector cables and a voltage amplifier to reach the PZTs. The PZTs are excited at different times to form a beam directed toward a specific target point at a specific angle. A schematic of the full experiment setup is seen in Figure 4.3. The points used for each angle are depicted in Figure 4.4, with the measured points located in quadrant I of the plate and 5 mm spacing between each measured point.

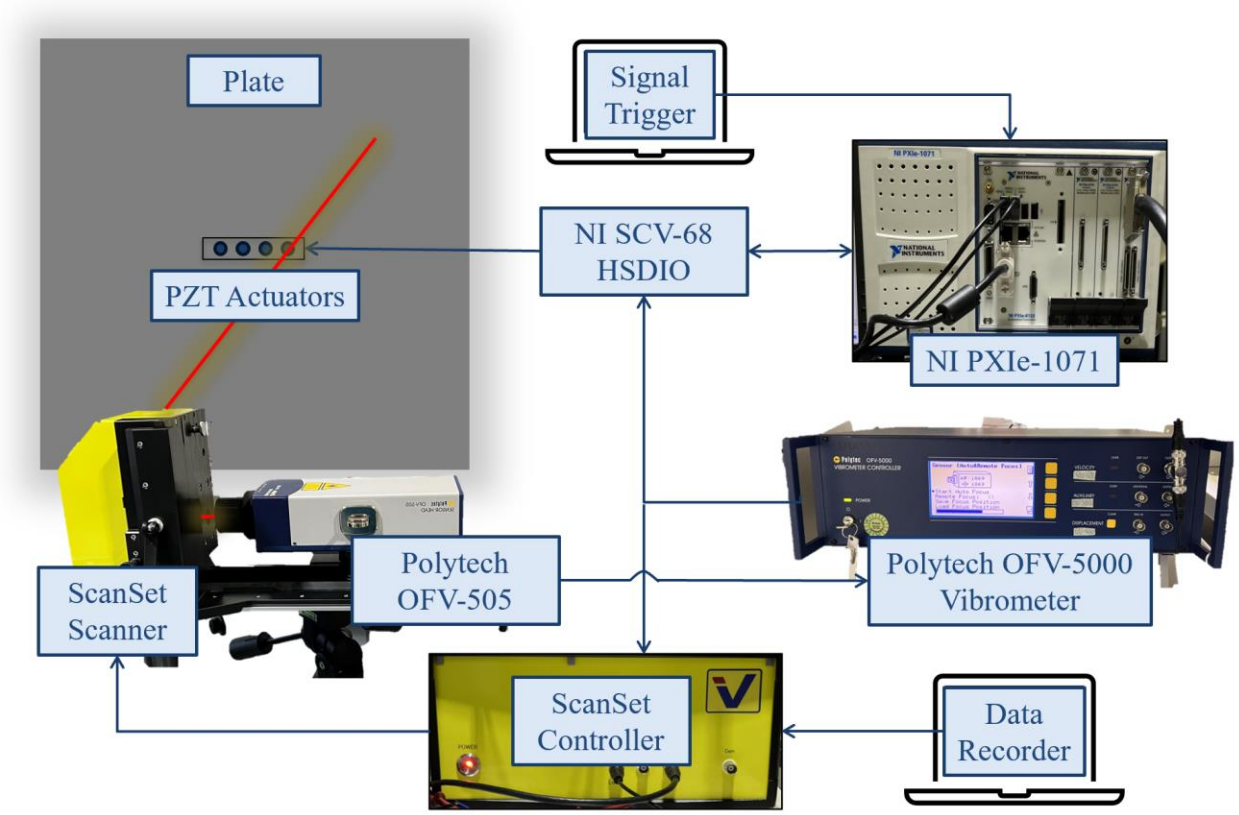

Figure 4.3 Experimental setup

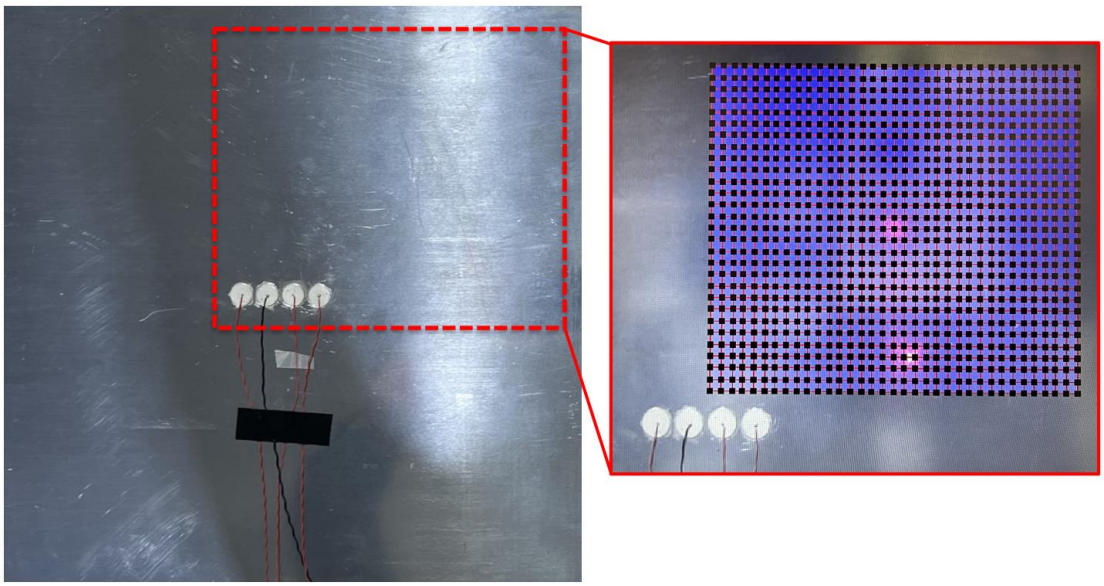

Figure 4.4 Aluminum plate and targeting points measured in quadrant I

When the signals are sent, the Polytech OFV-505 sensor head and OFV-5000 vibrometer controller capture the data from the out-of-plane velocity changes of the plate, employing VD-09.

The data is then directed back to the input channel of the National Instruments SCB-68 HSDIO and subsequently into the National Instruments NI PXIe-1071 via the NI PXI-7852R attachment.

4.2 Isotropic Case

The beamforming of 70° through the aluminum plate was successfully performed using a hybrid four-PZT actuator linear array and a laser vibrometer. An image of wave propagation through the plate, modeled by vibrometer data, is shown in Figure 4.5 Snapshot of moving 3D model of data showing wave. The x- and y-axes of Figure 4.5 are in mm, and the z-axis is in μm/s to indicate the velocity difference of a point on the panel.

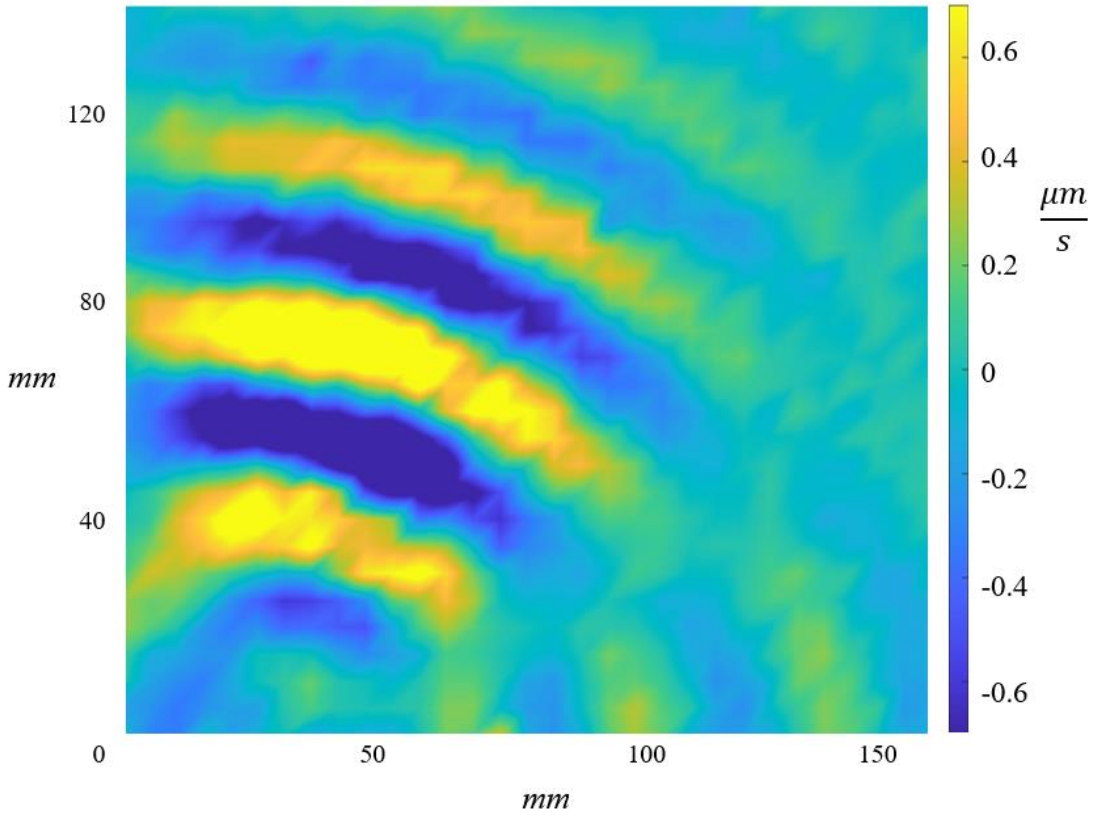

Figure 4.5 Snapshot of moving 3D model of data showing wave propagation through Aluminum plate

Error analysis was done to prove this model and the measurements were precise and not random. The standard deviation of each time interval for the 10 trials completed for every measured point on the plate was calculated. The mean of all the individual standard deviations for

the 70° beamformed angle was 91 $\mu m/s$. Further analysis of the data was done for five randomly selected points on the plate to see if the data across the 10 trials at each of those 5 positions matched. Analysis of Variance (ANOVA) two-factor without replication was used in Excel with a selected α at 0.05 for comparison for each of the 5 selected positions on the plate. In Table 4.2, the ANOVA data shows that for all 5 positions analyzed, the F-value is greater than the F-critical for the columns, where each trial is a column, and for the rows, where each row is a measurement of the trials at the same time-step. The main point of interest is the F-value is greater than the F-critical for the columns, indicating that the data gathered follows a pattern that is not random or erroneous from trial to trial of each measurement point on the plate.

Table 4.2 ANOVA Statistical Analysis of Random Measurement Points

Point	*Source of Variation*	*SS*	*df*	*MS*	*F*	*P-value*	*F crit*
(-32,160)	Rows	90000000	399	200000	40	<0.001	1
	Columns	20000000	9	2000000	300	<0.001	2
	Error	20000000	3591	7000			
	Total	100000000	3999				
(48,144)	Rows	300000000	399	600000	50	<0.001	1
	Columns	40000000	9	4000000	300	<0.001	2
	Error	50000000	3591	10000			
	Total	300000000	3999				
(48,112)	Rows	300000000	399	700000	200	<0.001	1
	Columns	300000	9	30000	8	<0.001	2
	Error	10000000	3591	4000			
	Total	300000000	3999				
(32,64)	Rows	300000000	399	600000	400	<0.001	1
	Columns	400000	9	50000	20	<0.001	2
	Error	7000000	3591	2000			
	Total	300000000	3999				
(128,48)	Rows	200000000	399	400000	100	<0.001	1
	Columns	700000	9	80000	20	<0.001	2
	Error	10000000	3591	4000			
	Total	200000000	3999				

4.3 Quasi-Isotropic Cases

The composite plates were tested using the same process as the isotropic case. For the AM composite panel at 60° targeting, Figure 4.6 shows the resulting wave propagation. Notice that the sidelobe in this panel is significantly more prominent in the composite panel than in the isotropic aluminum panel, which is to be expected.

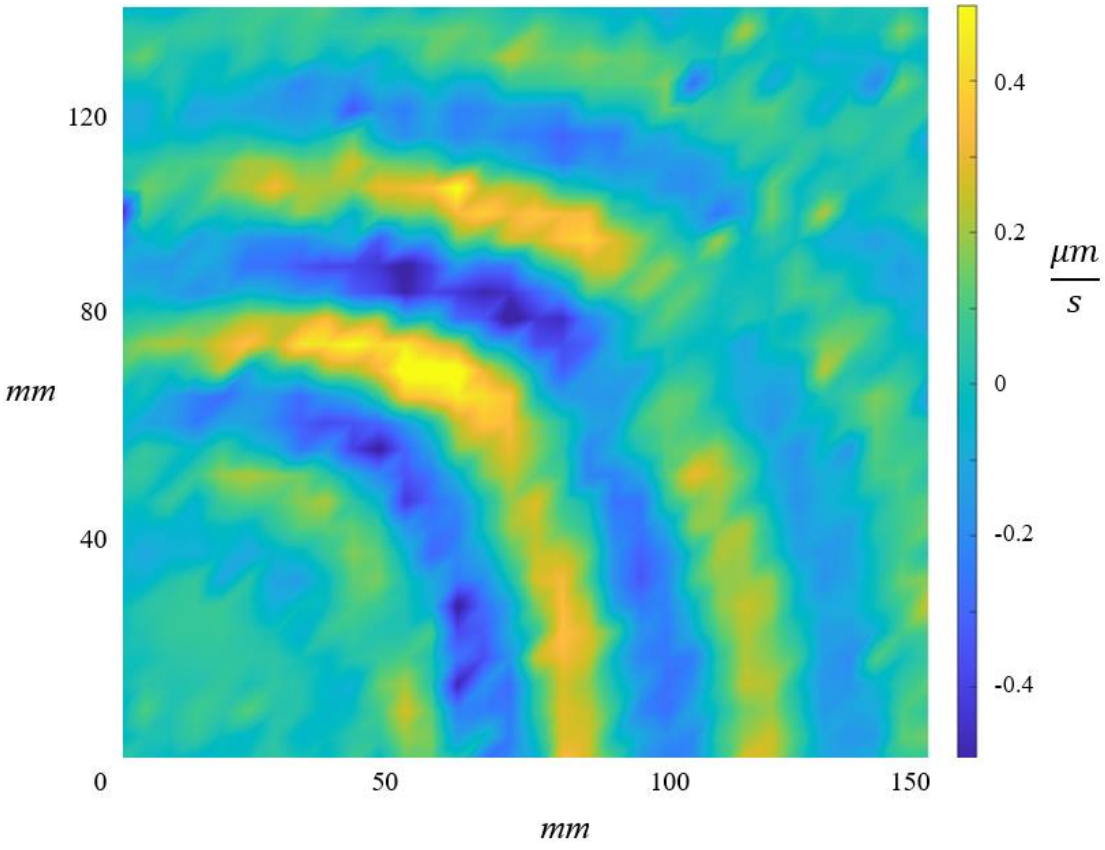

Figure 4.6 Snapshot of moving 3D model of data showing wave propagation through AM composite plate

Unfortunately, with the conventionally fabricated panel, it was difficult to get a good reading of the wave propagation. While similar methods were used across all samples, the surface of the panel was not as reflective as the other panels, and some equipment malfunctioned as data was being collected. Some conclusions were able to be drawn with the data collected and processing the results in Figure 4.7. Like the AM panel, the sidelobe is significantly more prominent than in

the isotropic panel. Additionally, since the panel is half as thick, the waves travel much more quickly through the panel. Due to this, a second slower refracted wave travel through the panel is observed, evident in the lower right quadrant of the snapshot.

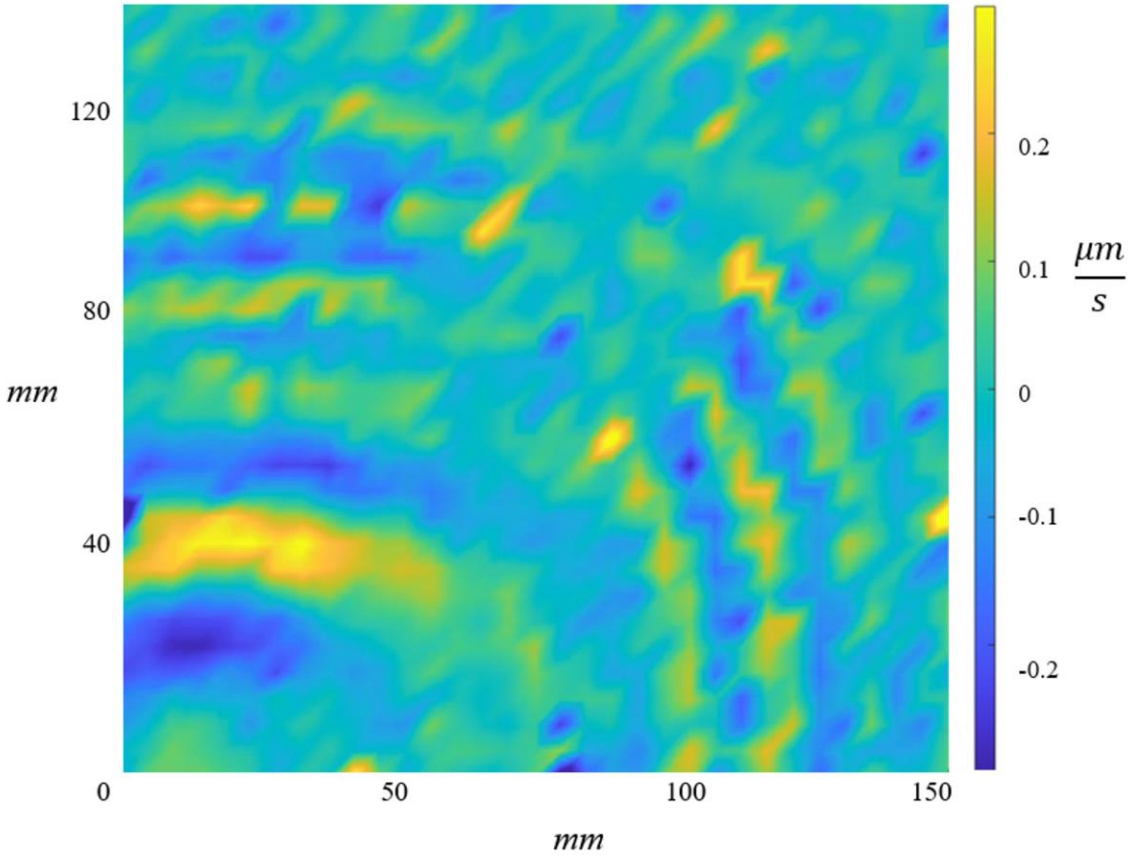

Figure 4.7 Snapshot of moving 3D model of data showing wave propagation through conventional composite plate

Additionally, in the conventional composite plate, beamforming was not able to successfully target past 75˚ angles. This is likely due to using such a small number of PZTs in the linear array tested. By increasing the number of PZTs, the useful range of the scan is increased as well.

4.4 Discussion

These results highlight the effectiveness of a combined system utilizing multiple PZT actuators and a laser vibrometer to generate a beamforming wave directed at specific angles. Rigorous error analysis and repeated trials were conducted to validate this system, ensuring precise and consistent

measurements. The experiment produced a 3D model depicting wave propagation across three distinct plates, clarifying the angles and directions at which the beam is directed. This provides valuable insight into how a beamsteered wave travels through various materials.

It's worth noting that variations in noise were observed in each scan, primarily due to differences in the reflective properties of the panels. The aluminum panel, with its mirror-like surface, exhibited less noise compared to the conventional composite panel, which appeared black and didn't reflect the laser back to the ScanSet Camera as effectively. To address this issue in future experiments, applying a thin layer of glossy clearcoat or metallic finish may help reduce noise levels. Additionally, due to the reflective nature of each panel, the peak amplitude recorded for each wave varied. Although it was expected that the thinner conventional composite panel would produce higher amplitude waves compared to the thicker AM composite panel, the opposite was observed. This can be attributed to the superior reflective quality of the AM panel. Notably, the aluminum plate displayed the most significant amplitude changes among all panels.

Also of note, there was some degree of educated guessing for the Elastic Modulus in both of the composite panels. Since the panels would be destroyed in order to determine the actual elastic modulus of both the printed and conventional composite panels, a number based on researched values was selected to utilize in the beamforming algorithm using the rule of mixtures, in the equation below, where E_F and E_m represent the elasticity modulus of the fiber and matrix and V_F and V_m represent the volume fraction of the fiber and matrix respectively.

$$E_c = E_F V_F + E_m V_m \tag{4.1}$$

Utilizing the exact value of the Elasticity Modulus of the composites instead of the estimated value would return more exact time delays to use for beamforming, and the experiments would see better beam steering towards the target.

Despite interference from noise and estimating the Young's Modulus, successful steering of the wave is observed to some degree in each of the three panels. Interestingly, despite the noise, wave propagation in both the AM and conventional composite panels appeared quite similar, with large sidelobes. However, slight deformation in the circular shape of the wave was observed in both composite panels, which can be attributed to the anisotropic nature of the material.

4.5 Damage Detection

To simulate damage, a slit was cut through the aluminum panel 10 cm away from the center of the array at a 60˚ angle. The scan was run again with a 60˚ beamsteering angle, with results in Figure 4.8.

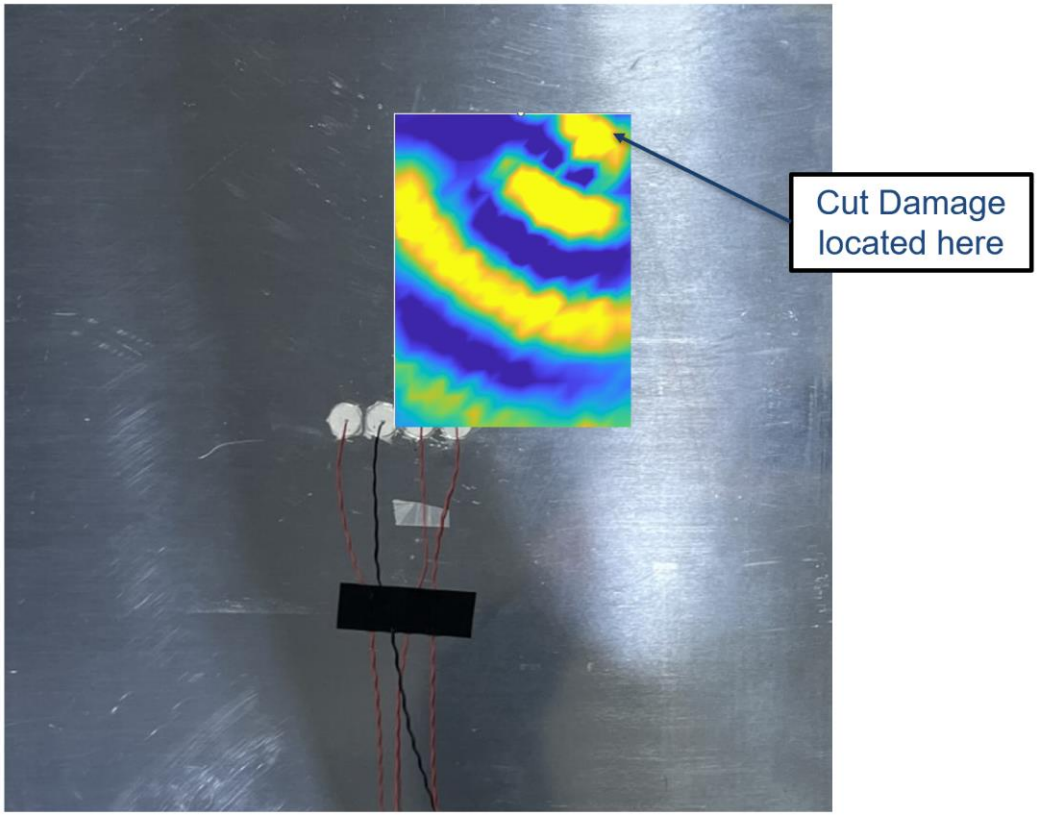

Figure 4.8 Scan of the Al panel shows the wave refraction caused by simulated damage

It is apparent that the wave is strongly reflected towards the PZTs. This demonstrates Lamb waves can propagate over large distances within a structure, allowing for extensive coverage,

which is particularly beneficial for monitoring large-scale components like aircraft wings or bridges.

5 Conclusions and Recommendations

This experimentation involves creating a 3D model to study the propagation of waves through different materials, including an Al 2024-T3C plate, an AM symmetric composite panel, and a conventional symmetric panel. It visualizes the angle and direction at which the beam is directed, enhancing our understanding of how beamsteered waves travel through diverse materials as the beam angle changes.

Advancements in research have elevated the readiness level of ultrasonic guided wave technology for monitoring the structural health of composite laminates. This technology can be further developed to incorporate AM components as advancements in AM and 3D printing emerge. By employing a phased array of sensors, it becomes possible to generate a controllable beam, effectively monitoring a significant area of an airframe structure. Detecting inter-ply delamination or fatigue damage allows for efficient planning and scheduling of maintenance activities.

This study experimentally establishes and demonstrates a structural health monitoring technique involving beamsteering Lamb waves through both metallic and composite panels. While research in beamsteering has not been explored in additive manufacturing prior to this study, it is shown that this SHM technique can be successfully applied to printed composite laminates.

5.1 Recommendations

Future work could improve and expand this research by making several key adjustments. First, by expanding the theoretical and numerical calculation of time delays to include quasi-isotropic panels. This would give more exact time delays for individual monitoring. Secondly, expand the experimentation to include additional configurations of composites, especially in additive manufacturing cases. This could be different printing resins, different carbon fiber content, etc.

Finally, additional angles of damage should be tested in other materials to determine the success rate of detection capabilities. Other types of damage could also be considered.

The author also recommends future research utilize more than four PZTs. This research was restricted to four PZTs due to the sample size of donated materials, but larger samples would allow a larger linear or 2D array, which would improve beamforming success and useful range.

6 REFERENCES

[1] Wang, L., and Yuan, F., "Group velocity and characteristic wave curves of lamb waves in composites: Modeling and experiments," *Composites Science and Technology*, vol. 67, 2007, 1370-1384.

[2] Valdes, S.H.D., and Soutis, C., "Real-time nondestructive evaluation of fiber composite laminates using low-frequency lamb waves," *Journal of the Acoustical Society of America*, vol.111, 2002, pp. 2023-2033.

[3] Wang, L., and Yuan, F., "Experimental study of lamp wave propagation in composite laminates," *Proceedings of SPIE*, 2006.

[4] Mancini, S., Tumino, G., and Gaudenzi, P., "Structural Health Monitoring for future Space Vehicles," *Journal of Intelligent Material Systems and Structures*, vol. 17, no. 7, 2006, pp. 577–585.
Doi: 10.1177/1045389X06059077

[5] Giurgiutiu, V.,"Structural health monitoring with piezoelectric wafer active sensors – predictive modeling and simulation," Incas Bull., vol. 2, no. 3, 2010, pp. 31–44.
Doi: 10.13111/2066-8201.2010.2.3.4

[6] Taylor, S.G., Raby, E. Y., Farinholt, K.M. Park, G., and Todd, M. D., "Active-sensing platform for structural health monitoring: Development and deployment," *Structural Health Monitoring*, vol. 15, no. 4, 2016, pp. 413–422.
Doi: 10.1177/1475921716642171

[7] de Oliveira, M. A., Monteiro, A. V., and Vieira Filho, J., "A new structural health monitoring strategy based on PZT sensors and Convolutional Neural Network," *Sensors*, vol. 18, 2018.

Doi: 10.3390/s18092955

[8] Kim, D., and Philen, M., “Guided Wave and Beamsteering using MFC Phased Arrays for Structural Health Monitoring: Analysis and Experiment,” *Journal of Intelligent Material Systems and Structures*, vol. 21, no. 10, 2010, pp. 1011-1024.
Doi: 10.1177/1045389X10372816

[9] Kim, D., "Phased Array Damage Detection and Damage Classification in Guided Wave Structural Health Monitoring." Dissertation, Virginia Tech, 2011.

[10] Staszewski, W. J., Mahzan, S., and Traynor, R., “Health monitoring of aerospace composite structures – Active and passive approach,” *Composites Science and Technology*, vol. 69, no. 11–12, 2009, pp. 1678–1685.
Doi: 10.1016/J.COMPSCITECH.2008.09.034.

[11] Lissenden, C., and Rose, J., “Structural health monitoring of composite laminates through ultrasonic guided wave beam forming,” *Nato applied vehicle technology symposium on military platform ensured availability proceedings*, 2008.

[12] Giurgiutiu, V., Zagrai, A., and Bao, J., “Damage identification in aging aircraft structures with piezoelectric wafer active sensors,” *Journal of Intelligent Material Systems and Structures*, vol. 15, 2004, pp. 673–687.
Doi: 10.1177/1045389X04038051

[13] Rose, J. L., *Ultrasonic guided waves in solid media*, New York, NY: Cambridge University Press, 2014.
Doi: 10.1017/CBO9781107273610

[14] Lin, B., and Giurgiutiu, V., "Modeling and testing of PZT and PVDF piezoelectric wafer active sensors," *Smart Materials and Structures*, vol. 15, no. 4, 2006, pp. 1085–1093.
Doi: 10.1088/0964-1726/15/4/022

[15] Giurgiutiu, V., Lin, B., Santoni-Bottai, G., and Cuc, A., "Space application of piezoelectric wafer active sensors for structural health monitoring," *Journal of Intelligent Material Systems and Structures*, vol. 22, no. 12, 2011, pp. 1359–1370.
Doi: 10.1177/1045389X11416029

[16] Giurgiutiu, V., Bao, J., and Zhao, W., "Piezoelectric wafer active sensor embedded ultrasonics in beams and plates," *Experimental Mechanics*, vol. 43, no. 4, 2003, pp. 428–449.
Doi: 10.1007/bf02411348

[17] Boukabache, H., Escriba, C., and Fourniols, J. Y., "Toward smart aerospace structures: Design of a piezoelectric sensor and its analog interface for flaw detection," *Sensors*, vol. 14, no. 11, 2014, pp. 20543–20561.
Doi: 10.3390/s141120543

[18] Ihn, J. B., and Chang, F. K., "Pitch-catch active sensing methods in structural health monitoring for aircraft structures," *Structural Health Monitoring*, vol. 7, no. 1, 2008, pp. 5–19.
Doi: 10.1177/1475921707081979

[19] Lissenden, C., and Rose, J., "Structural health monitoring of composite laminates through ultrasonic guided wave beam forming," *Nato applied vehicle technology symposium on military platform ensured availability proceedings*, 2008.

[20] Yu, L., & Giurgiutiu, V., "In-situ optimized PWAS phased arrays for lamb wave structural health monitoring," *Journal of Mechanics of Materials and Structures*, vol. 2, no. 3, 2007, pp. 459-487.

[21] Yu, L., and Giurgiutiu, V., "In situ 2-d piezoelectric wafer active sensors arrays for guided wave damage detection," *Ultrasonics*, vol.48, no.2, 2007, pp. 117-134.

[22] Wilcox, P., "Omni-directional guided wave transducer arrays for the rapid inspection of large areas of plate structures," *EEE Transactions on Ultrasonics, Ferroelectrics, and Frequency Control*, vol. 50, no. 6, 2003, pp. 699 - 709.

[23] Yu, L., and Tian, Z., "Lamb wave structural health monitoring using a hybrid PZT-laser vibrometer approach," *Structural Health Monitoring*, vol. 12, 2013, pp. 469–483.
Doi: 10.1177/1475921713501108

[24] Ning, F., Cong, W., Qiu, J., Wei, J., and Wang, S., "Additive manufacturing of carbon fiber reinforced thermoplastic composites using fused deposition modeling," *ASME Smart Materials, Adaptive Structures and Intelligent Systems*, vol. 80, 2015, pp. 369–378.
Doi: 10.1016/j.compositesb.2015.06.013

[25] Olmo, E. Grande, E. Samartin, C.R., Bezdenejnykh, M., Torres, J., Blanco, N., Frovel, M., and Cañas, J., "Lattice structures for aerospace applications," *12th European Conference on Space Structures, Materials, & Environmental Testing*, 2012.

[26] Peloquin, J., Han, Y., and Gall, K., "Printability and mechanical behavior as a function of base material, structure, and a wide range of porosities for polymer lattice

structures fabricated by VAT-based 3D printing," *Additive Manufacturing*, vol. 78, 2023, p. 103892.
doi: 10.1016/j.addma.2023.103892

[27] Zima, B., Kedra, R., "Numerical Study of Concrete Mesostructure Effect on Lamb Wave Propagation," *Ultrasound for Material Characterization and Processing*, vol. 13, no. 11, 2020, pp. 2570.
doi: 10.3390/ma13112570

[28] Rayleigh, J.W.S., *Theory of Sound*, New York: Dover, 1945.

[29] Wang, L., *Elastic wave propagation in composites and least-squares damage localization technique*, Unpublished master's thesis, Dept. Aerospace Engineering, North Carolina State University, 2004.

[30] Graff, K. F., *Wave motion in elastic solid*, Dover Publications, Inc., 1991.

[31] Nayfeh, A. H., *Wave propagation in layered anisotropic media: With application to composites*, North Holland, 1995.

[32] Osteric, P. Kim, D., and Yoo, B., "Phased array beamsteering in composite laminates for Guided Wave Structural Health Monitoring," *ASME Smart Materials, Adaptive Structures and Intelligent Systems*, vol. 2, 2013.
doi: 10.1115/SMASIS2013-3024

[33] Osteric, P., *Phased array beamsteering in composite laminates for guided wave structural health monitoring*, Unpublished master's thesis, Embry-Riddle Aeronautical University, 2015.

[34] Senyurek, V. Y., Baghalian, A., Tashakori, S., McDaniel, D., and Tansel, I. N., "Localization of multiple defects using the compact phased array (CPA) method," *Journal of Sound and Vibration*, vol. 413, 2018, pp. 383–394. doi: 10.1016/j.jsv.2017.10.037

[35] Demetgul, M., Senyurek, V. Y., Uyandik, R., Tansel, I. N., and Yazicioglu, O., "Evaluation of the health of riveted joints with active and passive structural health monitoring techniques," *Measurement*, vol. 69, pp. 42–51, 2015. doi: 10.1016/j.measurement.2015.03.032

[36] Rokhlin, S. I., Chimenti, D. E., and Nagy, P. B, *Physical ultrasonic of composites*, Oxford University Press, 2011.

[37] Lowe, M. J. S., "Matrix technique for modeling ultrasonic waves in multilayered media," *IEEE Transactions on Ultrasonics, Ferroelectrics, and Frequency Control*, vol. 42, no. 4, 1995, pp. 525-541.

[38] Kamal, A., and Giurgiutiu, V., "Stiffness transfer matrix method (stmm) for stable dispersion curves solution in anisotropic composites," *Proceedings of SPIE*, vol. 9064. 2014.

[39] Bhuiyan, M., Shen, Y., and Giurgiutiu, V., "Guided wave based crack detection in the rivet hole using global analytical with local FEM approach," *Materials*, vol. 9, 2016, p. 602. doi: 10.3390/MA9070602

[40] Monaco, E., Boffa, N. D., Maio, L., Ricci, F., Mendoza, E., Kundu, T., and Memmolo, V., "Hybrid guided wave based SHM system for composite structures for impact and delamination detection combining fiber Bragg grating sensing and

piezoelectric patches," *Health Monitoring of Structural and Biological Systems XII*, 2018.

doi: 10.31026/j.eng.2019.05.02

[41] Yu, L., and Giurgiutiu, V., "Damage detection using guided waves and piezoelectric wafer active sensor arrays," *Modal analysis conference; IMAC XXIV,* vol. 3, 2006, pp. 1202-1211.

[42] Rudolph, D., *Reduction of near-field grating loves in sparse acoustic phased arrays*, Unpublished master's thesis, Embry-Riddle Aeronautical University, 2013.